Structures, Energies, and Electrostatics for Methane Complexed with Alumina Clusters

Ellen F. Sawilowsky, Oussama Meroueh, H. Bernhard Schlegel, and William L. Hase*

Department of Chemistry, Wayne State University, Detroit, Michigan 48202-3489

Received: July 27, 1999; In Final Form: December 1, 1999

Ab initio calculations were used to investigate properties of complexes formed from the association of CH_4 with Al_2O_3, Al_4O_6, and Al_8O_{12} alumina clusters. Methane attaches to a surface Al atom of the cluster to form a complex with an Al−C separation that varies between 2.2 and 2.5 Å. The rotational motion for methane in these complexes is highly fluxional. Extrapolated G2MP2 well depths for the CH_4- - -Al_2O_3, CH_4- - -Al_4O_6, and CH_4- - -Al_8O_{12} complexes are 21, 14, and 17 kcal/mol, respectively. These different well depths are determined by the accessibility of the Al atom to which CH_4 binds and the size of the alumina cluster. The electrostatics of the three alumina clusters are very similar, with a charge on the surface Al atom of +2.2 to 2.3. The potential energy surface for a CH_4- - -$Al_{2n}O_{3n}$ cluster is represented semiquantitatively by an analytic function consisting of two-body potentials. The results of this study suggest that the adsorption energy for alkane molecules binding to alumina materials depends very strongly on the structure of the binding site.

I. Introduction

The properties of alumina (i.e., Al_2O_3) materials are of both technological and practical significance. Alumina is one of the most widely used ceramic materials.[1,2] It is used extensively in catalysts,[3] particularly those for hydrocarbon reactions,[4−6] and as dielectrics in microelectronics.[7] Adhesive bonds between aluminum oxide surfaces and polymers are widely used in the construction of lightweight materials and devices,[8,9] which have a wide range of applications. Alumina in the form of α- and γ-Al_2O_3 is one of the main constituents of rocket exhaust formed by solid propellant rocket motors (SRMs).[10] Al_2O_3 particles may provide sites for heterogeneous atmospheric chemistry and cloud nucleation.[11,12] The growing concentration of SRM alumina particles in the stratosphere[13] has raised concern about their potential impact on the ozone cycle.[12,14−16]

There have been numerous theoretical and experimental studies of the structures, energetics, and kinetics arising from materials interacting with alumina surfaces. The physi- and chemisorption of water with alumina surfaces has been studied theoretically by ab initio calculations,[17,18] and experimentally by high-temperature solution calorimetry,[19,20] laser-induced thermal desorption, and temperature-programmed desorption (TPD) techniques.[21,22] Experimental studies have addressed reactions of halomethanes[15,16] and perfluoroethers[23,24] with Al_2O_3 surfaces, the silation of alumina,[25] and the properties of di-*tert*-butyl nitroxide adsorbed on γ-Al_2O_3.[26]

Interfaces with alumina surfaces are of particular importance because they are integral parts of many devices. TPD has been used to investigate the desorption of alkane[27] and methanol[28] films from Al_2O_3. The surface force apparatus has been used to study the tribology of alumina surfaces[29] and the forces between alumina surfaces and aqueous sodium dodecyl sulfate surfactant solutions.[30] Semiempirical quantum chemical calculations have been used to explore adhesive interactions between acrylate and methylacrylate esters and Al_2O_3.[31] Molecular dynamics simulations have been performed to probe the temperature-dependent properties of silica/alumina[32] and water/alkane/alumina[33] interfaces.

Having an accurate description of adhesive interactions between alkanes and aluminum oxide would be very helpful for describing adhesion between polymers and alumina surfaces. However, there is considerable uncertainty regarding the energetics for alkane desorption from alumina surfaces.[27,34] TPD experiments[27] yield barriers of 8.4, 10.4, and 14.6 kcal/mol for desorption of butane, hexane, and octane, respectively, from an Al_2O_3 (0001) single crystal. These barriers are very similar to the bulk heats of sublimation for the alkanes.[27] In contrast, a model alkane/alumina potential energy function, derived from G2MP2 ab initio calculations for CH_4 interacting with the Al_2O_3 alumina cluster,[34] gives a 78 kcal/mol barrier for octane desorption from the aluminum-terminated surface of α-Al_2O_3 (0001). The ab initio calculations indicate this high barrier arises from strong electrostatic interactions between the C atoms of the alkane and the small aluminum cations of the surface, which have a charge of approximately +2.[34] The origin of this large difference between the experimental and theoretical alkane desorption barriers is unclear. The experimental alumina surface may be γ-Al_2O_3[19,20] and/or possibly oxygen-terminated or covered with a contaminant, given the high reactivity of the aluminum-terminated surface.[35]

In addition to the questions regarding the interactions of alkanes with the perfect α- and γ-alumina surfaces just presented, there are also uncertainties concerning alkane/alumina adhesive bonds for industrial materials.[36] Here the interface is not perfect, but characterized by significant imperfections such as pits, steps, kinks, protrusions, etc. It is expected that the strength of the alkane/alumina bond will be strongly affected by localized interactions at these defect sites.

In this paper, ab initio studies are reported for CH_4 interacting with the alumina clusters Al_4O_6 and Al_8O_{12}, which are compared with the previous calculations for the smaller cluster Al_2O_3. Of particular interest is determining how varying the size and structure of the $Al_{2n}O_{3n}$ cluster affects the nature of the CH_4- - -$Al_{2n}O_{3n}$ interaction and the electrostatics of the $Al_{2n}O_{3n}$ cluster. This information will help identify the manner in which the local alumina structure affects the strength of the alkane/alumina adhesive bond.
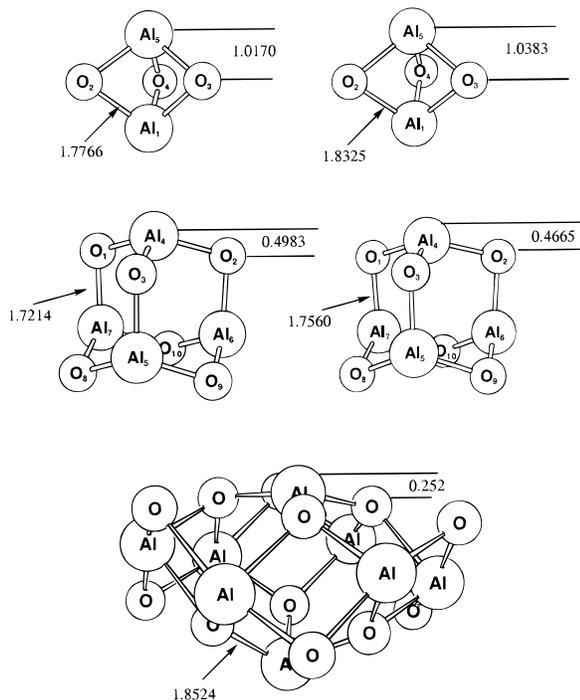
Properties of Methane−Alumina Clusters

J. Phys. Chem. A, Vol. 104, No. 21, 2000 **4921**

Figure 1. Optimized geometries for Al_2O_3 and Al_4O_6 at the HF/6-31+G(d) and MP2/6-31+G(d) levels of theory, and for Al_8O_{12} at the HF/6-31+G(d) level. The HF and MP2 geometries are on the left- and right-hand sides, respectively. The atom numbering for Al_8O_{12} is given in Figure 2.

Figure 2. Optimized geometries for the CH4- - -Al_2O_3 and CH4- - -Al_4O_6 complexes at the HF/6-31+G(d,p) and MP2/6-31+G(d,p) levels of theory, and for CH4- - -Al_8O_{12} at the HF/6-31+G(d,p) level. The HF and MP2 geometries are on the left- and right-hand sides, respectively.

Because of the long-range electrostatic properties of alumina, with its large Madelung constant,[37] the CH4- - -$Al_{2n}O_{3n}$ cluster systems studied here are too small to give the CH_4/alumina adsorption energy. It is expected that an $Al_{2n}O_{3n}$ cluster large enough to include all CH4- - -Al interactions extending over ∼20 Å or less is needed to converge the adsorption energy to within 1 kcal/mol.[33] However, the calculations are expected to assist in developing intermolecular potentials between the atoms of alkanes and alumina and to help test the alkane/alumina intermolecular potentials developed from the previous CH4- - -Al_2O_3 ab initio calculations.[34] These potentials may then be used to estimate the adsorption energies for alkanes bonding with different alumina surface structures. Previous electronic structure theory calculations for H_2O adsorbing on alumina[38] indicate that the CH4- - -$Al_{2n}O_{3n}$ cluster systems studied here will give meaningful structural information for CH_4 interacting with alumina surfaces. Cluster models have also been useful for studying reactions with diamond,[39-44] silicon,[45-47] and SiC surfaces.[48]

II. Properties OF $Al_{2n}O_{3n}$ Clusters and CH4- -$Al_{2n}O_{3n}$ Complexes

Three different aluminum oxide clusters were considered: Al_2O_3, Al_4O_6, and Al_8O_{12}. Optimized geometries were calculated by ab initio methods using the GAUSSIAN 94 and 98 series of programs.[49] Figure 1 shows the fully optimized geometries for the Al_2O_3 and Al_4O_6 clusters; the HF/6-31+G(d) and MP2/6-31+G(d) levels of theory give very similar results. The Al_8O_{12} cluster was constructed to model the surface of bulk aluminum oxide. As in our previous calculations,[17] the atoms of the surface AlO_3 group (atoms 1−4 in Figure 1) were represented by 6-31+G(d) basis functions and were fully optimized. The remaining atoms were represented by 3-21G basis functions and were frozen at the bulk Cartesian coordinates (obtained from the Cerius database).[50] The optimized Al−O_3(plane) spacing
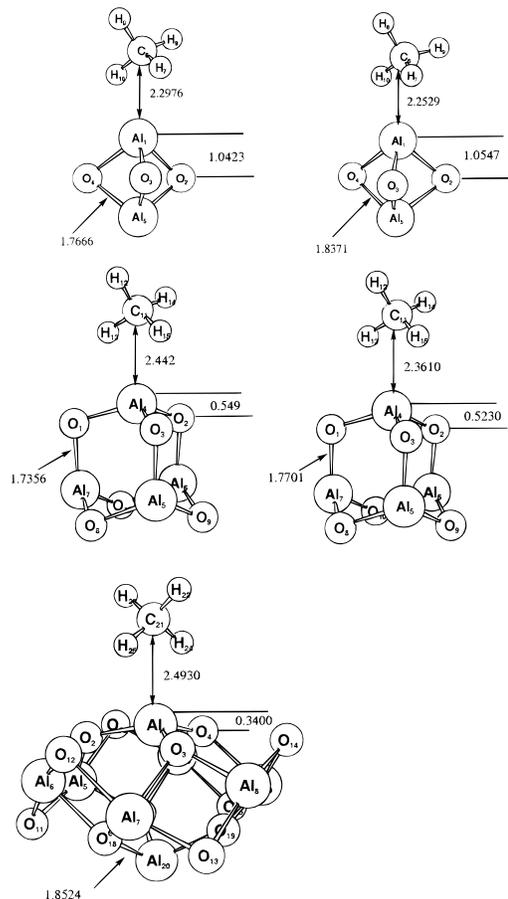
for this model, 0.25 Å,[17] agrees well with the experimental result, 0.3 ± 0.1 Å.[35]

The optimized geometries for methane interacting with the Al_2O_3, Al_4O_6, and Al_8O_{12} clusters are shown in Figure 2. The minimum energy structures have near C_s symmetry with the two H atoms pointing up and lying in a plane formed by one Al−O bond and the bisector of the O−Al−O angle of the other two O atoms. The C−H bonds pointing toward the cluster are slightly elongated (0.01−0.02 Å) and the surface Al is raised somewhat (0.02−0.09 Å relative to the corresponding distance without CH_4). By rotating CH_4, there are a total of 12 configurations for the minimum energy structure. For the CH4- - -Al_2O_3 complex, the barrier between these minima is only 0.05 kcal/mol at the HF/6-31+G(d) level, indicating that these complexes are highly fluxional.

Although molecular geometries are often described well at modest levels of theory, accurate binding energies and potential energy curves usually require higher levels of theory. To avoid complications arising from the fluxional character of these complexes, the CH4- - -$Al_{2n}O_{3n}$ clusters were constrained to have C_{3v} symmetry, with one hydrogen pointing away from the cluster and the remaining three hydrogens eclipsed with the oxygens. The high symmetry simplifies the geometry optimization and the fitting of the potential energy functions. However, the eclipsed C_{3v} structure is a second-order saddle point, 0.5−1.4 kcal/mol above the global C_s minimum and 0.1−0.6 kcal/mol below the staggered C_{3v} structure (a third-order saddlepoint). For the smallest cluster, levels of theory up to QCISD(T) and

TABLE 1: Binding Energies and Geometrical Parameters for the CH$_4$- -Al$_2$O$_3$ Complex[a]

theory	energy	Al—C	Al—O$_3$(plane)
HF/6-31G(d)	12.04	2.234	1.037
HF/6-31G(d,p)	12.75	2.220	1.038
HF/6-31+G(d)	12.49	2.220	1.042
HF/6-31+G(d,p)	13.21	2.206	1.043
HF/6-31++G(d,p)	13.25	2.206	1.043
B3LYP/6-31+G(d)	14.36	2.209	1.050
B3LYP/6-31+G(d,p)	14.95	2.198	1.050
B3LYP/6-31++G(d,p)	14.99	2.198	1.050
MP2/6-31+G(d)	16.99	2.171	1.056
MP2/6-31+G(d,p)	16.83	2.171	1.056
MP2/6-31++G(d,p)	16.95	2.170	1.056
HF/6-311+G(3df,2p)	16.31[b]		
MP2/6-311+G(3df,2p)	20.39[b]		
QCISD(T)/6-311G(d,p)	18.51[b]		
G2MP2	20.09[b]		

[a] C_{3v} geometry for CH$_4$ eclipsed with respect to the O atoms in the O$_3$(plane). [b] Using the MP2/6-31+G(d,p) optimized geometry.

G2MP2 were feasible, but for CH$_4$- - -Al$_8$O$_{12}$ only Hartree—Fock calculations were practical.

CH$_4$- - -Al$_2$O$_3$ Binding Energy. The effects of basis set and electron correlation on binding energy are shown in Table 1. Increasing the size of the basis from 6-31G(d) to 6-31++G-(d,p) increases the binding energy only ∼1 kcal/mol, with diffuse functions on hydrogen contributing very little. Changing from 6-31+G(d,p) to 6-311+G(3df,2p) increases the binding energy by 3–4 kcal/mol. Including electron correlation by second-order Møller—Plesset perturbation theory (MP2) increases the binding energy by 3–4 kcal/mol, whereas using density functional theory increases the binding energy by <2 kcal/mol. Improving the treatment of electron correlation by employing the QCISD-(T) level of theory instead of MP2 changes the energy by <0.4 kcal/mol with the 6-311G(d,p) basis. The MP2/6-311+G(3df,-2p) binding energy is within 0.4 kcal/mol of the G2MP2 calculations, which represents the best level of theory used in the present work. For the largest basis set, 6-311+G(3df,2p), the HF energy is within 4 kcal/mol and 80% of the G2MP2 value, which illustrates the importance of both polarization functions and electron correlation for the CH$_4$- - -Al$_2$O$_3$ interaction energy. By contrast, the effects of basis set and correlation on the geometry are small (0.06 Å for the Al—C separation, 0.02 Å for the Al—O$_3$(plane) separation). If the MP2/6-31+G-(d,p) calculations are used for the difference between the eclipsed C_{3v} structure and C_s global minimum (0.75 kcal/mol), the binding energy for global minimum is estimated to be 20.8 kcal/mol at the G2MP2 level of theory.

When an H atom of CH$_4$ points toward the aluminum, the CH$_4$- - -Al$_2$O$_3$ binding energy is much smaller. With CH$_4$ and Al$_2$O$_3$ constrained in their monomer optimized geometries and adopting a C_{3v} eclipsed configuration, the HF/6-31G(d), HF/6-311+G(3df,2p), and G2MP2 binding energies for the C—H—Al orientation are 0.42, 4.9, and 7.04 kcal/mol, respectively.

The effect of basis set superposition error (BSSE) was investigated using the counterpoise method.[51] With the HF/6-31+G(d,p) basis, this correction lowered the binding energy by 2.20 kcal/mol, a 16% effect.

CH$_4$- - -Al$_4$O$_6$ Binding Energy. Table 2 lists the binding energies for various levels of theory for this complex. Inspection of Figure 2 shows that CH$_4$- - -Al$_4$O$_6$ has a longer Al—C separation than CH$_4$- - -Al$_2$O$_3$, in accord with a much weaker binding energy. As will be shown later, the principal origin of this effect is the significantly shorter Al—O$_3$(plane) separation for Al$_4$O$_6$. Electron correlation effects are slightly larger than

TABLE 2: Binding Energies and Geometrical Parameters for the CH$_4$- -Al$_4$O$_6$ Complex[a]

theory	energy	Al—C	Al—O$_3$(plane)
HF/6-31G(d,p)	6.15	2.420	0.540
HF/6-31+G(d)	5.45	2.434	0.546
HF/6-31+G(d,p)	5.81	2.405	0.548
HF/6-311+G(d)	6.28	2.398	0.559
B3LYP/6-31+G(d,p)	8.07	2.319	0.529
B3LYP/6-31++G(d,p)	8.23	2.318	0.529
MP2/6-31+G(d,p)	10.47	2.302	0.525

[a] C_{3v} geometry for CH$_4$ eclipsed with respect to the O atoms in the O$_3$(plane).

for CH$_4$- - -Al$_2$O$_3$, increasing the binding energy by 4.6 kcal/mol and decreasing the Al—C distance by 0.1 Å at the MP2 level. The CH$_4$- - -Al$_4$O$_6$ complexes are also very fluxional: the C_{3v} structures listed in Table 2 are second-order saddlepoints, and the C_s global minimum shown in Figure 2 is 0.8 kcal/mol lower in energy. Comparison of these results with CH$_4$- - -Al$_2$O$_3$ indicates that the G2MP2 binding energy could be ∼14 kcal/mol.

CH$_4$- - -Al$_8$O$_{12}$ Binding Energy. At the HF/6-31+G(d,p) level, the binding energy is 8.81 kcal/mol for the eclipsed C_{3v} structure and 10.21 kcal/mol for the near C_s global minimum (shown in Figure 2). Comparison of these results with CH$_4$- - -Al$_2$O$_3$ and CH$_4$- - -Al$_4$O$_6$ suggests that the G2MP2 binding energy may be as much as 17 kcal/mol. The Al—C separation is ∼0.08 Å longer and the Al—O$_3$(plane) separation is ∼0.2 Å smaller for CH$_4$- - -Al$_8$O$_{12}$ than for CH$_4$- - -Al$_4$O$_6$. The staggered C_{3v} structure is slightly lower than the eclipsed. Interestingly, though the Al atom is closer to the O$_3$(plane) for Al$_8$O$_{12}$ than for Al$_4$O$_6$, the former has a larger CH$_4$ binding energy, which may arise from a greater number of Al atoms interacting with CH$_4$ (see analysis later).

Effect of the Al—O$_3$(Plane) Separation. The calculations just presented suggest that the binding energy for CH$_4$ and the alumina cluster is influenced by the distance the Al atom sits above the O$_3$ plane; that is, the Al—O$_3$(plane) separation. This property was investigated in more detail for each of the three complexes, by setting the Al—O$_3$(plane) separation to the values found for the three optimized clusters. Because of the highly fluxional character of the CH$_4$- - -Al$_{2n}$O$_{3n}$ complexes with respect to the orientation of CH$_4$, the effect of the Al—O$_3$(plane) separation may be investigated by considering any one of the optimized configurations for CH$_4$ with respect to the alumina cluster. For convenience and to be systematic, CH$_4$ was constrained in its optimized geometry and fixed in an eclipsed, C_{3v} configuration with respect to the O$_3$(plane) of the cluster. This arrangement eliminated any possible small effects from using different CH$_4$ orientations for the three CH$_4$- - -Al$_{2n}$O$_{3n}$ systems. This C_{3v} orientation for CH$_4$ was also used for calculations of the charges and potential energy curves presented next.

The results in Table 3 show how changing the Al—O$_3$(plane) separation affects properties of the CH$_4$- - -Al$_{2n}$O$_{3n}$ complexes. For each of the clusters, "pulling up" the Al atom and increasing the Al—O$_3$(plane) separation results in a larger CH$_4$ binding energy. This effect could arise from a greater positive charge on the Al atom and/or reduced repulsions between the O atoms of the cluster (principally those in the O$_3$ plane) when the aluminum atom is pulled up. The relative importance of these two possibilities is considered later. Table 3 also shows that, for a fixed Al—O$_3$(plane) separation, the CH$_4$ binding energy increases as the size of the alumina cluster is increased. Apparently, the overall attractive interaction between CH$_4$ and alumina cluster becomes larger with more atoms in the cluster.

Properties of Methane−Alumina Clusters

J. Phys. Chem. A, Vol. 104, No. 21, 2000 **4923**

TABLE 3: Binding Energies and Al−C Distances, and Al Atom Charges for Constrained CH$_4$- -Al$_{2n}$O$_{3n}$ Complexes^a

	Al$_2$O$_3$			Al$_4$O$_6$			Al$_8$O$_{12}$		
Al−O$_3$(plane) separation	energy	Al−C	q	energy	Al−C	q	energy	Al−C	q
0.252^b	0.955	3.213	1.73	1.64	3.022	2.16	7.79	2.663	2.20
0.498^c	2.75	2.671	1.92	4.61	2.514	2.22	12.70	2.353	2.22
1.017^d	11.37	2.251	2.13	14.77	2.197	2.27	21.13	2.148	2.24

^{a} Calculations at the HF/6-31+G(d,p) level of theory with an eclipsed, C_{3v} geometry for the complex. Both CH$_4$ and the Al$_{2n}$O$_{3n}$ clusters are constrained in their HF/6-31+G(d,p) optimized geometry, except for two of the calculations for each cluster where the top Al atom is "pulled up" or "pushed down" to attain the specified Al−O$_3$(plane) separation. ^{b} Al−O$_3$(plane) separation for the optimized Al$_8$O$_{12}$ cluster. ^{c} Al−O$_3$(plane) separation for the optimized Al$_4$O$_6$ cluster. ^{d} Al−O$_3$(plane) separation for the optimized Al$_2$O$_3$ cluster.

TABLE 4: Natural Population Analysis Charges for the Cluster Models^a

element	Al$_2$O$_3$	Al$_4$O$_6$	Al$_8$O$_{12}$	CH$_4$- - -Al$_2$O$_3$	CH$_4$- - -Al$_4$O$_6$	CH$_4$- - -Al$_8$O$_{12}$
Al, surface	2.22	2.27	2.30	2.11	2.19	2.20
O, surface	−1.48	−1.51	−1.62	−1.47	−1.51	−1.62
Al, bulk^b	2.22	2.27	- -	2.20	2.26	- -
O, bulk^b	- -	−1.51	- -	- -	−1.51	- -
C	- -	- -	- -	−1.00	−0.97	−0.95
H^c	- -	- -	- -	0.31, 0.25	0.28, 0.24	0.27, 0.23

^{a} Calculated at the HF/6-31+G(d,p) level for the optimized geometries shown in Figures 1 and 2. For isolated CH$_4$, the charges of the C and H atoms are −0.90 and 0.22, respectively. ^{b} Average charge for the bulk atoms. The bulk atoms in Al$_8$O$_{12}$ and CH$_4$- - -Al$_8$O$_{12}$ were represented by the 3-21G basis set and their charges are not reported. ^{c} The larger charges are for the two H atoms pointing up.

Electrostatics. Alumina clusters are known to be highly ionic.[17] Table 4 compares the natural population analysis charges for Al$_{2n}$O$_{3n}$ and CH$_4$- - -Al$_{2n}$O$_{3n}$. The surface atoms are those in the Al−O$_3$(plane) group and the remaining atoms comprise the bulk. The charges are only weakly dependent on cluster size, with a small increase in the atomic charges of the surface atoms as the size of the cluster increases. Binding of CH$_4$ decreases the charge on the surface Al by ∼0.1, but has almost no effect on the other charges. Pulling the surface Al atom up from the O$_3$ plane in the Al$_4$O$_6$ cluster changes the surface Al and O charges by 0.09 and −0.07, respectively, but does not change the other charges significantly; the changes are even smaller for CH$_4$- - -Al$_4$O$_6$ (0.03 and 0.00, respectively). Figure 3 shows that the charges are fairly constant as the Al−C distance is elongated. Only when CH$_4$ is pushed hard into the cluster do the charges on the surface atoms change significantly. The implication is that a model with fixed charges on the atoms of the alumina cluster may be suitable for the thermal 300 K dynamics of the CH$_4$- - -Al$_{2n}$O$_{3n}$ complexes.

III. Potential Energy Functions

Long-Range Potential. The $1/r^n$ long-range potentials for CH$_4$ interacting with Al$_2$O$_3$ and Al$_4$O$_6$ were calculated at the HF/6-31+G(d,p) level of theory, with CH$_4$ and the alumina clusters constrained in their optimized geometries and CH$_4$ fixed in an eclipsed, C_{3v} orientation with respect to the O$_3$ plane of the cluster. The results are plotted in Figure 4 in logarithmic form, where ln(V) and ln(r) equal the logarithms of the CH$_4$− alumina cluster potential and of the Al−C separation, respectively. The slope of a plot of ln(V) versus ln(r) equals $-n$. Slopes of the curves are determined for r in the ranges 3−5 and 6−10 Å. For the CH$_4$- - -Al$_2$O$_3$ curve, n equals 5.0 and 5.9 for the inner and outer r intervals, respectively. The outer n is near the expected value of 6 for the long-range CH$_4$- - -Al$_2$O$_3$ quadrupole−octopole interaction.[52] The value of n is 5.2 for r in the complete 3−10 Å range. For CH$_4$- - -Al$_4$O$_6$, n = 4.4 for r in the 3−5 Å range and n = 6.8 for r in the 6−10 Å range. The value of n for the complete curve, r = 3−10 Å, is 5.2. The value of n for the outer range of r values is consistent with n = 7 for the CH$_4$- - -Al$_4$O$_6$ octopole−octopole interaction.[52]

HF and Analytic Potential Curves. Complete potential energy curves for CH$_4$ interacting with the Al$_4$O$_6$ and Al$_8$O$_{12}$
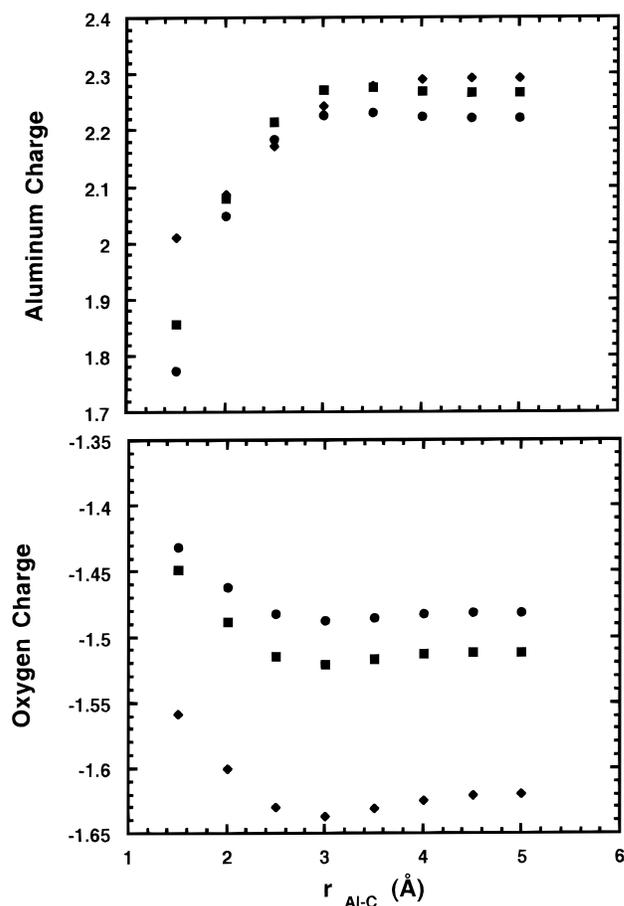

Figure 3. Charges of the Al and O surface atoms as a function of the Al−C separation for the CH$_4$- - -Al$_{2n}$O$_{3n}$ complexes. The charges are from a natural population analysis at the HF/6-31+G(d,p) level of theory. CH$_4$ and Al$_{2n}$O$_{3n}$ are constrained in their monomer optimized geometries and CH$_4$ is in an eclipsed, C_{3v} orientation with respect to the surface O$_3$(plane). Key: (○) CH$_4$- - -Al$_2$O$_3$; (□) CH$_4$- - -Al$_4$O$_6$; and (◇) CH$_4$- - -Al$_8$O$_{12}$.

clusters, with both the attractive and repulsive components, are plotted in Figure 5. Each curve was computed at the HF/6-31+G(d,p) level of theory, with the geometries of both CH$_4$ and the alumina cluster fixed and CH$_4$ constrained to a C_{3v}
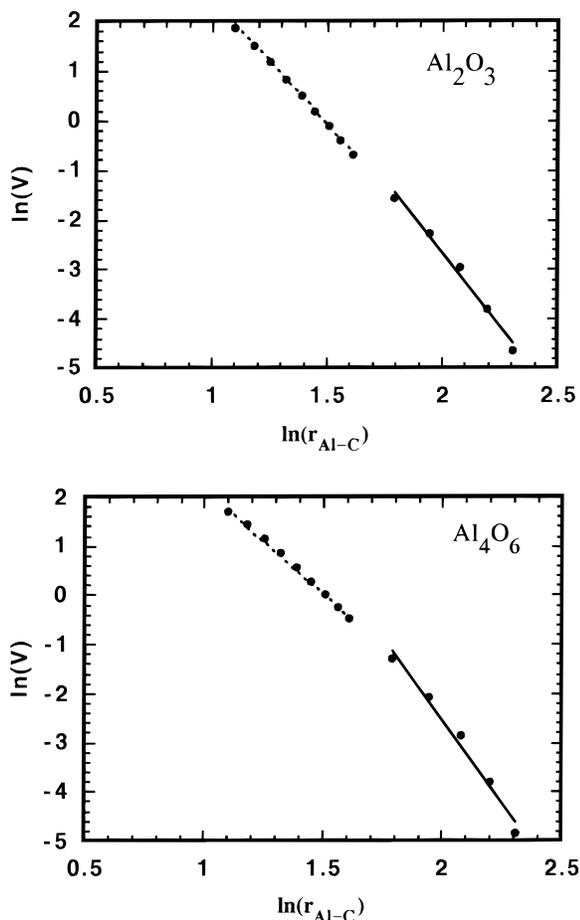
4924 *J. Phys. Chem. A, Vol. 104, No. 21, 2000*

Sawilowsky et al.

Figure 4. Plots of ln V versus ln r for CH$_4$- - -Al$_2$O$_3$ and CH$_4$- - - Al$_4$O$_6$ potentials at the MP2/6-31+G(d,p) level of theory: CH$_4$ is in an eclipsed, C_{3v} orientation with respect to the surface O$_3$(plane), V is in kcal/mol, and r is in Å. The dashed lines are fits to the curves for r of 3−5 Å and the solid lines are the fits for r of 6−10 Å.

eclipsed configuration with respect to the O$_3$(plane). For each alumina cluster, the upper curve is for the cluster fixed in its optimized monomer geometry and the lower curve for a modified geometry where the surface Al atom "pulled up" so that the Al−O$_3$(plane) separation is 1.043 Å (the value for the optimized CH$_4$- - -Al$_2$O$_3$ complex).

It is possible to simultaneously fit these four curves for CH$_4$- - -Al$_4$O$_6$ and CH$_4$- - -Al$_8$O$_{12}$ with a sum of two-body potentials between the C atom of methane and the Al and O atoms of the clusters; that is,

$$V = \sum_i [a_o \exp(-b_o r_i) - c_o/r_i^6 - d_o/r] +$$
$$\sum_i [a_{Al} \exp(-b_{Al} r_i) - c_{Al}/r_i^6 - d_{Al}/r] \quad (1)$$

where the first summation is for C- - -O interactions and the latter for the C- - -Al interactions. These fits are represented by the solid lines in Figure 5. The parameters are $a_o = 12\,626$ kcal/mol, $b_o = 2.0652$ Å^{-1}, $c_o = 12\,515$ kcal-Å^6/mol, $d_o = 16.838$ kcal-Å/mol, $a_{Al} = 3.1426 \; 10^5$ kcal/mol, $b_{Al} = 4.2015$ Å^{-1}, $c_{Al} = 6108.6$ kcal-Å^6/mol, and $d_{Al} = -25.845$ kcal-Å/mol. This potential is an approximate united-atom (UA) model for CH$_4$ interacting with an alumina clusters, which does not include averaging over the CH$_4$ orientations. An obvious shortcoming of this model is that the hydrogen atoms of CH$_4$ are not treated explicitly. However, it is significant that the model simultaneously fits CH$_4$ interactions with both Al$_4$O$_6$ and Al$_8$O$_{12}$. In the next section, additional potential energy curves

TABLE 5: Parameters for Fits to the CH$_4$- -Al$_4$O$_6$ HF/ 6-31+G(d,p) Potential Energy Curves

interaction	parameter[a]			
	a	b	c	d
Al−C	1.5423×10^5	4.6017	-1.0817×10^3	−138.10
Al−H	4.2923×10^4	4.4335	-4.9857×10^2	22.550
O−C	4.0611×10^3	2.5907	8.0370×10^2	58.279
O−H	8.1759×10^2	2.5361	1.5292×10^1	−6.4640

[a] The respective units for the parameters a, b, c, and d are kcal/mol, Å^{-1}, kcal-Å^6/mol, and kcal-Å/mol.

are analyzed for the CH$_4$- - -Al$_4$O$_6$ system in an attempt to derive a potential with explicit hydrogen atoms.

HF and Analytic Potential Energy Surfaces. The potential energy curves in Figure 5 are for CH$_4$- - -Al$_{2n}$O$_{3n}$ interactions along the H−C−Al C_{3v} symmetry axis. To develop a more general potential, which explicitly includes the H atoms, three additional potential energy curves at the HF/6-31+G(d,p) level of theory were calculated for the CH$_4$- - -Al$_4$O$_6$ system. For each curve, CH$_4$ and Al$_4$O$_6$ were held fixed in their individual optimized geometries. The three curves are for an H atom approaching an Al atom along the C−H−Al C_{3v} axis, the C atom approaching an O atom along the H−C−O C_{2v} axis, and an H atom approaching an O atom along the C−H−O C_{2v} axis. These three potential curves, along with the two in Figure 5 for CH$_4$- - -Al$_4$O$_6$, are plotted in Figure 6.

The best simultaneous fit to these five potential energy curves is shown in Figure 6, with the potential energy function in eq 1 used to represent Al−C, Al−H, O−C, and O−H two-body interactions. The parameters are listed in Table 5. Though the fit to these curves is not quantitative, overall it is quite good given the range of interactions represented. An obvious limitation of the potential energy function is the inclusion of only two-body terms and neglect of higher-order terms.

Scaling the HF Potential Energy Surface. MP2/6-31+G-(d,p) potential curves, as a function of the Al−C separation, are given in Figure 7 for the CH$_4$- - -Al$_4$O$_6$ system. For these curves, the geometries of CH$_4$ and Al$_4$O$_6$ are fixed, with CH$_4$ constrained to a C_{3v}, eclipsed configuration with respect to the O$_3$(plane). The two curves differ in the geometry of Al$_4$O$_6$ as for the HF/6-31+G(d,p) curves in Figure 5: for one, Al$_4$O$_6$ is fixed in its optimized monomer geometry, for the other, the surface Al atom is "pulled up" so that the Al−O$_3$(plane) separation is 1.043 Å. There are considerable differences between the depths of the HF and MP2 potential energy curves, V_0 (HF) and V_0(MP2), respectively. For the optimized Al$_4$O$_6$ structure, the respective HF and MP2 well depths are 4.61 and 8.85 kcal/mol. These depths are 15.20 and 17.88 kcal/mol respectively, with the Al atom "pulled-up." Figure 7 shows that if the HF curve is scaled by the factor V_0(MP2)/V_0(HF), a very good representation of the MP2 curve results. The curves are plotted versus $r - r_{min}$, where r_{min} is the Al−C separation at the potential energy minimum. The HF and MP2 r_{min} values are 2.442 and 2.361 Å, respectively, for the optimized Al$_4$O$_6$ cluster. These values are shorter, 2.191 and 2.173 Å, respectively, for the cluster with the Al atom pulled-up.

For the deeper set of potential energy curves, the Al atom is pulled-up and the interaction is dominated by Al- - -C electrostatics; accordingly, the V_0(MP2)/V_0(HF) scale factor is only 1.176. However, for the optimized Al$_4$O$_6$ cluster, the Al atom is less exposed and, thus, electrostatics are less dominant. As a result, electron correlation becomes more important and the scale factor increases considerably to 1.919. The dependence of the scaling on the Al atom binding site suggests it will be difficult
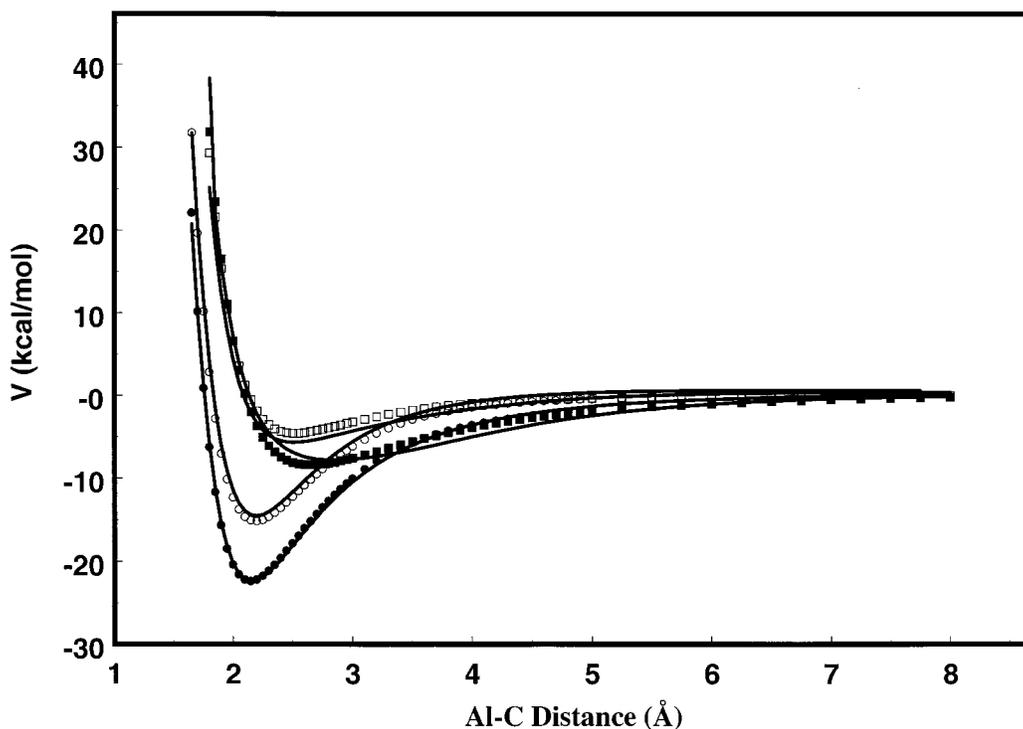
Properties of Methane−Alumina Clusters

J. Phys. Chem. A, Vol. 104, No. 21, 2000 **4925**

Figure 5. HF/6-31+G(d,p) potential energy curves for the CH$_4$- - -Al$_4$O$_6$ and CH$_4$- - -Al$_8$O$_{12}$ systems, versus the Al−C separation. Key: (square) the alumina cluster is fixed in its optimized monomer geometry; (circle) the alumina cluster has this geometry with the surface Al pulled up so that the Al−O$_3$(plane) separation is 1.043 Å (the open symbols are for Al$_4$O$_6$ and the closed symbols are for Al$_8$O$_{12}$). The CH$_4$ is constrained to its optimized monomer geometry, with an eclipsed, C_{3v} configuration with respect to the AlO$_3$ surface atoms. The fits (solid lines) are given by eq 1.
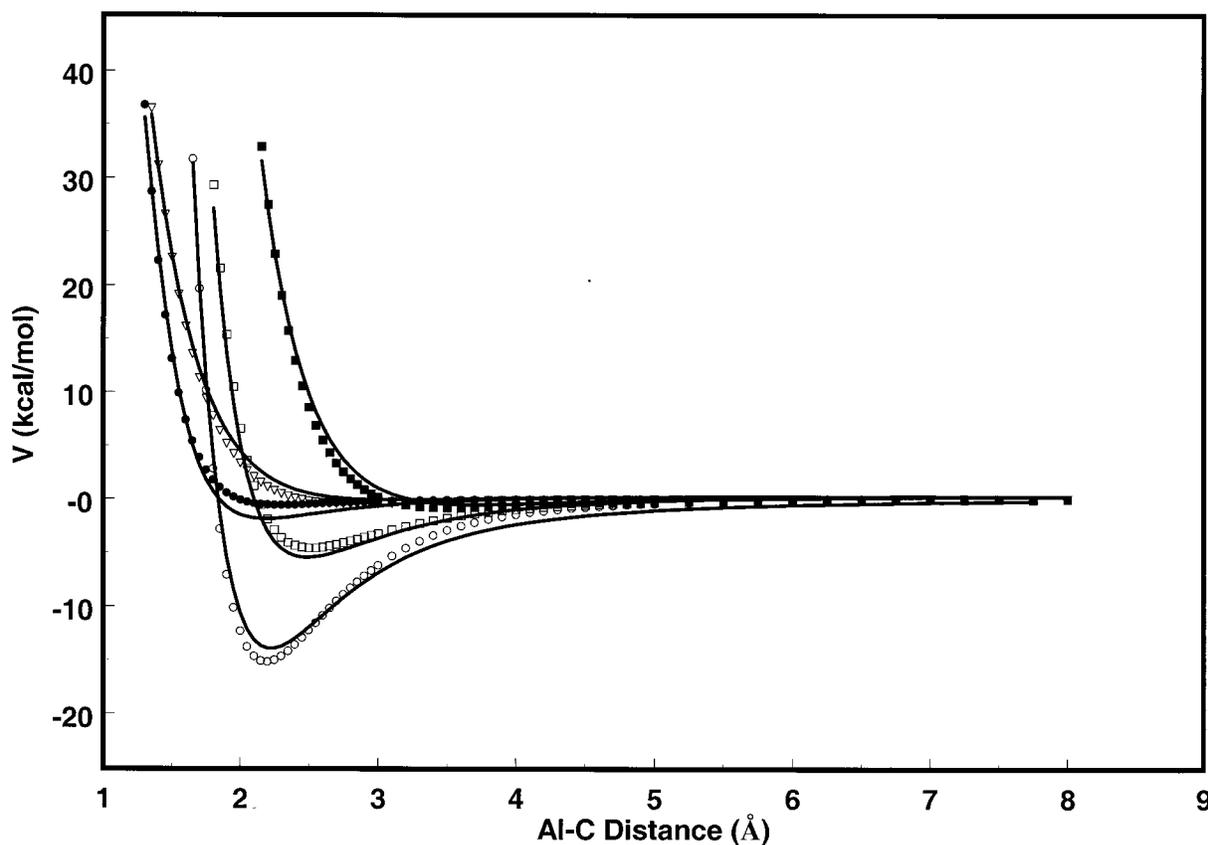

Figure 6. HF/6-31+G(d,p) potential curves for CH$_4$- - -Al$_4$O$_6$. Key: (O) and (□) are the same as in Figure 5; (●) an H atom approaches an Al atom along the C−H−Al C_{3v} axis; (■) the C atom approaches an O atom along the H−C−O C_{2v} axis; (∇) an H atom approaches an O atom along the C−H−O C_{2v} axis. The solid lines are a fit with a sum of 2-body potentials (see text).

to develop an accurate potential energy surface for methane interacting with alumina clusters by scaling an HF surface to

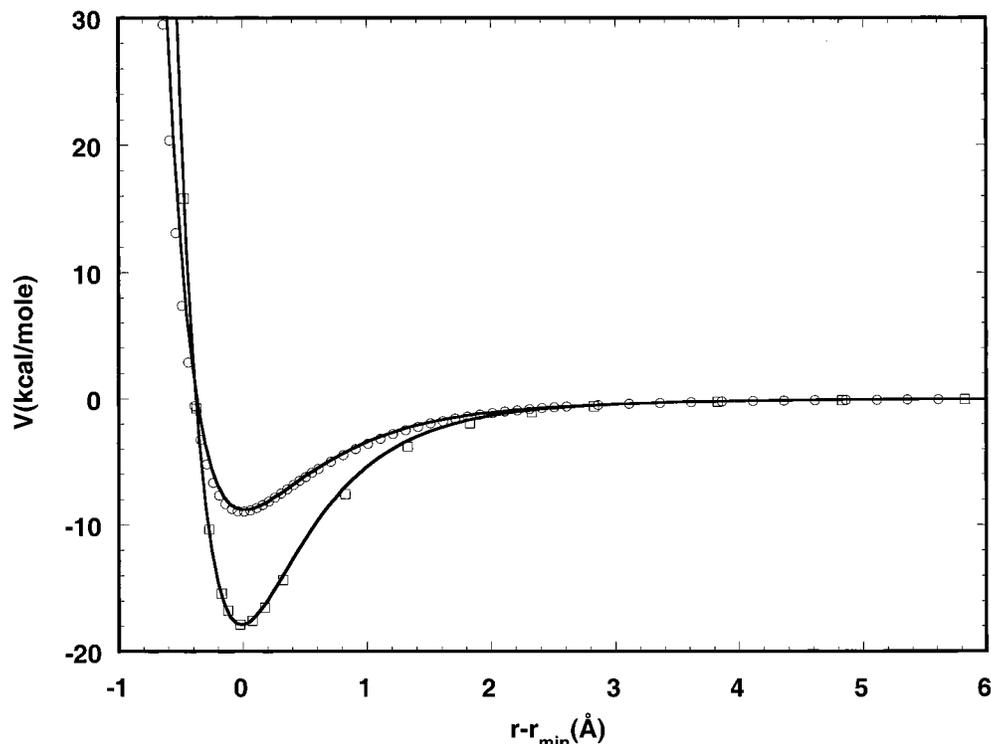match potential energy minima for a much higher level of theory.

Figure 7. Comparison of (—) scaled HF/6-31+G(d,p) and (○ and □) MP2/6-31+G(d,p), potential energy curves for CH_4- - -Al_4O_6 versus the Al—C separation. The HF curves in Figure 5 for CH_4- - -Al_4O_6 are scaled by the relative MP2 and HF well depth for each curve [i.e., $V_0(MP2)/V_0(HF)$]. The symbols have the same meaning as in Figure 5: (○) optimized cluster; (□) Al—O_3(plane) separation is 1.043 Å. For the Al_4O_6 cluster with the Al-atom pulled up, r_{min} is 2.191 and 2.173 Å at the HF and MP2 levels, respectively.

IV. Summary

The methane molecule in the CH_4- - -$Al_{2n}O_{3n}$ complexes interacts with and attaches to one of the exterior small Al cations of the alumina cluster. The distance between the C atom and this Al atom varies between 2.2 and 2.5 Å for the three optimized complexes. The C—Al bond is shortened when the Al atom is pulled out from the cluster and lengthened when it is pushed in. Though there is a rather strong interaction between CH_4 and $Al_{2n}O_{3n}$, rotational motions of CH_4 in each complex are highly fluxional, with very little change in potential energy as CH_4 attains different orientations with respect to the $Al_{2n}O_{3n}$ cluster. Methane is well described as a weak hindered rotor with respect to the alumina cluster.

The well depths, for the optimized complexes formed by CH_4 binding to Al_2O_3, Al_4O_6, and Al_8O_{12}, are 14.1, 6.6, and 10.2 kcal/mol, respectively, at the HF/6-31+G(d,p) level of theory. This well depth for CH_4- - -Al_2O_3 is 70% of the 20.8 kcal/mol well depth found at the G2MP2 level theory, the highest level of theory considered in this work. If the 6-311+G(3df,2p) basis set is used in the HF calculation for CH_4- - -Al_2O_3, the resulting well depth is 80% of the G2MP2 value. This result illustrates the importance of electrostatics for the CH_4—alumina cluster interaction, but electron correlation must also be treated to obtain quantitative energetics.

The different values of the well depths for the optimized CH_4- - -Al_2O_3, CH_4- - -Al_4O_6, and CH_4- - -Al_8O_{12} complexes arise from the extent that the Al atom to which CH_4 binds is separated from the remaining atoms in the alumina cluster and the size of the cluster. Increasing this separation increases the binding energy. These results suggest that the adsorption energy for methane or other alkane molecules binding to alumina surface will depend very strongly on the structure of the binding site (e.g., a terrace, ledge, pit, protrusion, etc) and the availability of the Al cation. This dependence is observed experimentally

for zeolites,[53-55] where the Al atoms are somewhat concealed in occluded tetrahedral sites.[56] Alkanes, ranging in size from methane to hexane, bind to zeolites with a small number of nonframework cations, with adsorption energies of 5 to 14 kcal/mol in the zero coverage limit.[53-55]

The electrostatics of the Al_2O_3, Al_4O_6, and Al_8O_{12} clusters are very similar. The charge of a surface Al atom is 2.2 to 2.3. An O atom in the O_3(plane) beneath this Al has a charge of -1.5 to -1.6. The charge of the surface Al atom changes by only a small amount, ~ 0.1, when CH_4 binds. Significant changes in the electrostatics of the cluster occur only when CH_4 is pushed into the cluster. These findings suggest that a model with fixed charges on the atoms of the alumina cluster may adequately describe the thermal dynamics of CH_4- - -$Al_{2n}O_{3n}$ complexes.

The binding energies found here between CH_4 and the Al_4O_6 and Al_8O_{12} clusters support the ab initio results presented previously[34] for the CH_4- - -Al_2O_3 system. From this latter study, 78 kcal/mol is predicted for the energy of desorption of octane from the Al-terminated α-Al_2O_3(0001) surface. For the Al_8O_{12} cluster, the separation between the surface Al atom and the neighboring O_3(plane) is 0.25 Å and nearly the same as the experimental result[35] of 0.3 ±0.1 Å for the Al-terminated α-Al_2O_3(0001) surface. Thus, this cluster models the surface structure. At the HF/6-31+G(d,p) level of theory, the CH_4- - -Al_8O_{12} binding energy is 10.2 kcal/mol. Calculations for the CH_4- - -Al_2O_3 system show that this level of theory gives a binding energy that is 70% of the G2MP2 value. Using this correction gives a G2MP2 binding energy of 15 kcal/mol for CH_4- - -Al_8O_{12}. If each CH_3 and CH_2 moiety of an octane molecule interacts with an Al atom on the alumina surface with this binding energy, the octane/Al-terminated α-Al_2O_3(0001) desorption energy would be 112−120 kcal/mol. However, the $CH_3(CH_2)$ groups of the octane do not align directly above the surface Al atoms[33,34] and a lower desorption energy will result.

Properties of Methane−Alumina Clusters

J. Phys. Chem. A, Vol. 104, No. 21, 2000 **4927**

It is noteworthy that this ab initio octane/Al-terminated α-Al₂O₃-(0001) desorption energy is considerably larger than the experimental desorption energies of 8−15 kcal/mol for butane, hexane, and octane on an Al₂O₃(0001) surface.[27] As discussed previously,[34,35] the surface used in these experiments may not be Al terminated.

The feasibility of using two-body potentials between the atoms of CH_4 and $Al_{2n}O_{3n}$ to represent ab initio potentials for CH_4- - -$Al_{2n}O_{3n}$ complexes was explored for the CH_4- - -Al_4O_6 system. A sum of two-body potentials of the form [a exp($-br$) $- c/r^6 - d/r$] was found to give an overall good fit to a set of HF/6-31+G(d,p) potential energy curves for CH_4- - -Al_4O_6 with a range of interactions. In future work it will be important to extend such a fit to ab initio calculations at a higher level of theory that more accurately treats electron correlation. It will also be important to include a range of CH_4- - -$Al_{2n}O_{3n}$ complexes in the fit so that the resulting potential is a general one for $Al_{2n}O_{3n}$ alumina clusters of different sizes. Until this is done, the most reliable potential for CH_4- - -$Al_{2n}O_{3n}$ complexes is that derived from G2MP2 calculations for CH_4- - -Al_2O_3.[34]

References and Notes

(1) Gitzen, W. H. *Alumina as a Ceramic Material*; American Ceramic Society: Columbus, OH, 1970.

(2) Dörre, E.; Hübner, H. *Alumina: Processing, Properties, and Applications*; Springer: Berlin, 1984.

(3) Knozinger, H.; Ratnasamy, P. *Catal. Rev. Sci. Eng.* **1978**, *17*, 31.

(4) Verykios, X. E.; Stein, F. P.; Coughlin, R. W. *Catal. Rev. Sci. Eng.* **1980**, *22*, 197.

(5) McCabe, R. W.; Mitchell, P. S. *J. Catal.* **1987**, *103*, 419.

(6) Yomaoa, M.; Yasumaro, J.; Hovalia, M.; Hercules, D. M. *J. Phys. Chem.* **1991**, *95*, 7037.

(7) Gautier, M.; Renaud, G.; Van, L. P.; Villette, B.; Pollak, M.; Thromat, N.; Jollet, F.; Duraud, J.-P. *J. Am. Ceram. Soc.* **1994**, *77*, 323.

(8) Kinloch, A. J. *Adhesion and Adhesives: Science and Technology*; Chapman and Hall: London, 1987.

(9) Lee, L. H., Ed. *Fundamentals of Adhesion*; Plenum: New York, 1991.

(10) Laredo, D.; McCrorie, J. D., III; Vaughn, J. K.; Netzer, D. W. *J. Propul. Power* **1994**, *10*, 410.

(11) Turco, R. P.; Toon, O. B.; Whitten, R. C.; Cicerone, R. J. *Nature* **1982**, *298*, 830.

(12) Robinson, G. N.; Freedman, A.; Kolb, C. E.; Worsnop, D. R. *Geophys. Res. Lett.* **1994**, *21*, 377.

(13) Zolensky, M. E.; McKay, D. S.; Kaczor, L. A. *J. Geophys. Res.* **1989**, *94*, 1047.

(14) Jackman, C. H.; Considine, D. B.; Fleming, E. L. *J. Geophys. Res.* **1996**, *101*, 12523.

(15) Dai, Q.; Robinson, G. N.; Freedman, A. *J. Phys. Chem. B* **1997**, *101*, 4940.

(16) Robinson, G. N.; Dai, Q.; Freedman, A. *J. Phys. Chem. B* **1997**, *101*, 4947.

(17) Wittbrodt, J. M.; Hase, W. L.; Schlegel, H. B. *J. Phys. Chem. B* **1998**, *102*, 6539.

(18) Hass, K. C.; Schneider, W. F.; Curioni, A.; Andreoni, W. *Science* **1998**, *282*, 265.

(19) McHale, J. M.; Navrotsky, A.; Perrotta, A. J. *J. Phys. Chem. B* **1997**, *101*, 603.

(20) McHale, J. M.; Auroux, A.; Perrotta, A. J.; Navrotsky, A. *Science* **1997**, *277*, 788.

(21) Elam, J. W.; Nelson, C. E.; Cameron, M. A.; Tolbert, M. A.; George, S. M. *J. Phys. Chem. B* **1998**, *102*, 7008.

(22) Nelson, C. E.; Elam, J. W.; Cameron, M. A.; Tolbert, M. A.; George, S. M. *Surf. Sci.* **1998**, *416*, 341.

(23) Lyth, E.; Ng, L. M. *J. Phys. Chem.* **1995**, *99*, 17615.

(24) Meyers, J. M.; Desrosiers, R. M.; Cornaglia, L.; Gellman, A. *J. Trib. Lett.* **1998**, *4*, 155.

(25) Slavov, S. V.; Sanger, A. R.; Chuang, K. T. *J. Phys. Chem. B* **1998**, *102*, 5475.

(26) Katter, U. J.; Hill, T.; Risse, T.; Schlienz, H.; Beckendorf, M.; Klüner, T.; Hamann, H.; Freund, H.-J. *J. Phys. Chem. B* **1997**, *101*, 552, 3776.

(27) Slayton, R. M.; Aubuchon, C. M.; Camis, T. L.; Noble, A. R.; Tro, N. J. *J. Phys. Chem.* **1995**, *99*, 2151.

(28) Nishimura, S. Y.; Gibbons, R. F.; Tro, N. J. *J. Phys. Chem. B* **1998**, *102*, 6831.

(29) Berman, A.; Steinberg, S.; Campbell, S.; Ulman, A.; Israelachvili, J. *Trib. Lett.* **1998**, *4*, 43.

(30) Xu, Z.; Ducker, W.; Israelachvili, J. *Langmuir* **1996**, *12*, 2263.

(31) Hulubka, J. W.; Dickie, R. A.; Cassatta, J. C. *J. Adhesion Sci. Technol.* **1992**, *6*, 243.

(32) Blonski, S.; Garofalini, S. H. *J. Phys. Chem.* **1996**, *100*, 2201.

(33) de Sainte Claire, P.; Hass, K. C.; Schneider, W. F.; Hase, W. L. *J. Chem. Phys.* **1997**, *106*, 7331.

(34) Bolton, K.; Bosio, S. B. M.; Hase, W. L.; Schneider, W. F.; Hass, K. C. *J. Phys. Chem. B* **1999**, *103*, 3885.

(35) Ahn, J.; Rabalais, J. W. *Surf. Sci.* **1997**, *388*, 121.

(36) Lee, L. H. *Adhesion* **1994**, *46*, 15.

(37) Douglas, B. E.; McDaniel, D. H. *Concepts and Models of Inorganic Chemistry*; Ginn: Toronto, 1965.

(38) DFT/BLYP calculations for an extended supercell model of the α-Al₂O₃(0001) surface[18] and HF, MP2, and B3LYP calculations based on cluster models of the surface[17] give similar structures for the molecular and dissociation adsorption of water and for the dissociative adsorption transition state.

(39) Besler, B. H.; Hase, W. L.; Hass, K. C. *J. Phys. Chem.* **1992**, *96*, 9369.

(40) Weiner, B.; Skokov, S.; Frenklach, M. *J. Chem. Phys.* **1995**, *102*, 5486; Frenklach, M.; Skokov, S. *J. Phys. Chem. B* **1997**, *101*, 3025.

(41) Pederson, M. R.; Jackson, K. A.; Pickett, W. E. *Phys. Rev. B* **1991**, *44*, 3891.

(42) Redfern, P. C.; Horner, D. A.; Curtiss, L. A.; Gruen, D. M. *J. Phys. Chem.* **1996**, *100*, 11654.

(43) Brown, R. C.; Cramer, C. J.; Roberts, J. T. *J. Phys. Chem. B* **1997**, *101*, 9574.

(44) Larsson, K.; Carlsson, J.-O.; Lunell, S. *Phys. Rev. B* **1995**, *51*, 10 003; Carbone, M.; Larsson, K.; Carlsson, J.-O. *J. Phys. Chem. B.* **1997**, *101*, 9445.

(45) Shoemaker, J. R.; Burggraff, L. W.; Gordon, M. S. *J. Phys. Chem. B*, in press; Shoemaker, J. R.; Burggraff, L. W.; Gordon, M. S. *J. Chem. Phys.* **2000**, *112*, 2994.

(46) Nachtigall, P.; Jordan, K. D.; Sosa, C. *J. Chem. Phys.* **1994**, *101*, 8073; Smith, A. P.; Wiggs, J. K.; Jonsson, H.; Yan, H.; Corrales, L. R.; Nachtigall, P.; Jordan, K. D. *J. Chem. Phys.* **1995**, *102*, 1044.

(47) Penev, E.; Kratzer, P.; Scheffler, M. *J. Chem. Phys.* **1999**, *110*, 2986.

(48) Choi, C. H.; Gordon, M. S. submitted for publication in *J. Am. Chem. Soc.*

(49) Frisch, M. J.; Trucks, G. W.; Schlegel, H. B.; Scuseria, G. E.; Robb, M. A.; Cheeseman, J. R.; Zakrzewski, V. G.; Montgomery, J. A.; Stratmann, R. E.; Burant, J. C.; Dapprich, S.; Millam, J. M.; Daniels, A. D.; Kudin, K. N.; Strain, M. C.; Farkas, O.; Tomasi, J.; Barone, V.; Cossi, M.; Cammi, R.; Mennucci, B.; Pomelli, C.; Adamo, C.; Clifford, S.; Ochterski, J.; Petersson, G. A.; Ayala, P. Y.; Cui, Q.; Morokuma, K.; Malick, D. K.; Rabuck, A. D.; Raghavachari, K.; Foresman, J. B.; Cioslowski, J.; Ortiz, J. V.; Stefanov, B.; Liu, G.; Liashenko, A.; Piskorz, P.; Komaromi, I.; Gomperts, R.; Martin, R. L.; Fox, D. J.; Keith, T.; Al-Laham, M. A.; Peng, C. Y.; Nanayakkara, A.; Gonzalez, C.; Challacombe, M.; Gill, P. M. W.; Johnson, B. G.; Chen, W.; Wong, M. W.; Andres, J. L.; Head-Gordon, M.; Replogle, E. S.; Pople, J. A. *Gaussian 98*; Gaussian, Inc.: Pittsburgh, PA, 1998, and earlier versions.

(50) *Cerius2*; BIOSYM/Molecular Simulations: San Diego, CA, 1995.

(51) Boys, S. F.; Bernardi, F. *Mol. Phys.* **1970**, *19*, 533; Tao, F. M.; Pan, Y. K. *J. Phys. Chem.* **1991**, *95*, 3582.

(52) Berry, S. R.; Rice, S. A.; Ross, J. *Physical Chemistry*; John Wiley: New York, 1980; p 408.

(53) Silva, J. A. C.; Rodrigues, A. E. *Ind. Eng. Chem. Res.* **1997**, *36*, 493.

(54) Silva, J. A. C.; Rodrigues, A. E. *AIChE* **1997**, *43*, 2524.

(55) Savitz, S.; Siperstein, F.; Gorte, R. J.; Myers, A. L. *J. Phys. Chem. B* **1998**, *102*, 6865.

(56) Cotton, F. A.; Wilkinson, G. *Advanced Inorganic Chemistry, 2nd Ed.*; John Wiley: New York, 1966; p 473.